
Letter

A new formation scenario of a counter-rotating circumstellar disk: spiral-arm accretion from a circumbinary disk in a triple protostar system

Daisuke TAKAISHI,^{1,*} Yusuke TSUKAMOTO,^{1,*} and Yasushi SUTO^{2,3,*}

¹Graduate School of Science and Engineering, Kagoshima University, Kagoshima 890-0065, Japan

²Department of Physics, The University of Tokyo, Tokyo 113-0033, Japan

³Research Center for the Early Universe, School of Science, The University of Tokyo, Tokyo 113-0033, Japan

*E-mail: k3790238@kadai.jp, tsukamoto.yusuke@sci.kagoshima-u.ac.jp, suto@phys.s.u-tokyo.ac.jp

Received 2021 April 23; Accepted 2021 August 3

Abstract

We present the evolution of rotational directions of circumstellar disks in a triple protostar system simulated from a turbulent molecular cloud core with no magnetic field. We find a new formation pathway of a counter-rotating circumstellar disk in such triple systems. The tertiary protostar forms via the circumbinary disk fragmentation and the initial rotational directions of all the three circumstellar disks are almost parallel to that of the orbital motion of the binary system. Their mutual gravito-hydrodynamical interaction for the subsequent $\sim 10^4$ yr greatly disturbs the orbit of the tertiary, and the rotational directions of the tertiary disk and star are reversed due to the spiral-arm accretion of the circumbinary disk. The counter-rotation of the tertiary circumstellar disk continues to the end of the simulation ($\sim 6.4 \times 10^4$ yr after its formation), implying that the counter-rotating disk is long-lived. This new formation pathway during the disk evolution in Class 0/I Young Stellar Objects possibly explains the counter-rotating disks recently discovered by ALMA.

Key words: protoplanetary disks — hydrodynamics — methods: numerical

1 Introduction

Unprecedented recent high angular resolution and sensitivity of the Atacama Large Millimeter/submillimeter Array (ALMA) have revealed many surprising discoveries. Counter-rotating circumstellar disks in young close binary systems are such examples. For instance, the O-type proto-binary system IRAS 16547–4247, of which a projected separation is 300 au, hosts counter-rotating twin disks (Tanaka et al. 2020). Young binary and multiple systems also frequently have circumstellar disks of which

the rotational directions are misaligned with each other, with that of the circumbinary/circum-multiple disk, and with the orbital plane (e.g., Jensen & Akeson 2014; Brinch et al. 2016; Takakuwa et al. 2017; Alves et al. 2019; Kraus et al. 2020; Ichikawa et al. 2021).

While the counter-rotating disks are discovered, the origin has not been completely clarified from the point of view of the formation process. Previous theoretical studies have suggested two major scenarios of the binary and multiple formation: the turbulent fragmentation and the disk fragmentation. The turbulent fragmentation naturally ex-

plains the counter-rotating and/or misaligned disks at the formation epoch (e.g., Fisher 2004; Offner et al. 2010). This possible formation process of the primordial counter-rotating and/or misaligned disks, however, prefer the large separation of > 500 au (Offner et al. 2010). The IRAS 16547–4247 has the apparent separation of 300 au, and the disk fragmentation scenario is more preferable (e.g., Adams et al. 1989; Bonnell & Bate 1994). However, it has been believed that the counter-rotating disks are difficult to form by the disk fragmentation so far because it tends to form the initially well-aligned disks.

This letter reports a new scenario for the counter-rotating disk formation in a triple protostar system that forms by the disk fragmentation; a tertiary circumstellar disk evolves into a counter-rotating disk by the spiral-arm accretion of the circumbinary disk.

2 Outline of our SPH simulation

We consider a triple protostar system, model C3, listed in Table 1 of our previous paper (Takaishi et al. (2020), hereafter Paper I). Paper I describes details of the numerical simulation. Therefore, we briefly present the numerical simulation here.

We perform a set of systematic simulation runs of the isolated turbulent molecular cloud core collapse using three-dimensional smoothed particle hydrodynamics (SPH) with $N_p = 10^6$ particles. The magnetic field is not considered in the simulation. The formation and evolution of a protostar are represented by the sink particle (Bate et al. 1995), which is dynamically created when the density of an SPH particle exceeds the threshold density $\rho_{\text{sink}} = 4 \times 10^{-8} \text{ g cm}^{-3}$ (see section 2.1 in Paper I).

The simulation starts from a cloud core approximated by an isothermal uniform gas sphere with the initial temperature of $T_{\text{init}} = 10 \text{ K}$, the mass of $M_{\text{init}} = 1 M_{\odot}$, and the radius of $R_{\text{init}} = 3.9 \times 10^3 \text{ au}$. The initial turbulent velocity field corresponds to the mean Mach number of $\mathcal{M} = 0.67$, and its velocity power spectrum is proportional to k^{-4} (Burkert & Bodenheimer 2000), where k is the wavenumber. Paper I focused on the evolution of the spin-orbit angles of isolated circumstellar disk systems, and model C3 is one of the two triple systems generated in Paper I (see their section 2.2 and Table 1).

3 Formation and evolution of a counter-rotating circumstellar disk

The simulation is conducted from the cloud core collapse to $t_{\text{ps1}} = 82,000 \text{ yr}$, where t_{ps1} is the elapsed time after the primary protostar (ps1) formation. First, ps1 forms at

$\sim 49,000 \text{ yr}$ after the beginning of the cloud core collapse. Then, the secondary protostar (ps2) forms at $t_{\text{ps1}} = 940 \text{ yr}$ by the disk fragmentation. Finally, the tertiary protostar (ps3) forms at $t_{\text{ps1}} = 17,700 \text{ yr}$ because of the spiral-arm fragmentation in the circumbinary disk by the gravitational instability.

Figure 1 shows the evolution of the surface density of the triple system, during which the rotational direction of the tertiary circumstellar disk (csd3) is reversed in the evolution.¹ **Panels (a)-(c):** the rotational direction of csd3 is counter-clockwise and the same as that of the primary circumstellar disk (csd1), secondary circumstellar disk (csd2), and the orbital motion of the binary system. Three circumstellar disks, csd1, csd2, and csd3, approximately orbit on the x - y plane. **Panels (c)-(f):** the orbit of csd3 becomes eccentric, and csd3 starts crossing the circumbinary disk. Therefore, the gas component of csd3 is disturbed and partially stripped. **Panels (g)-(j):** csd3 develops by the spiral-arm accretion of the circumbinary disk, resulting that the rotational direction of csd3 is reversed (from counter-clockwise to clockwise) and opposite as that of csd1, csd2, and the orbital motion of the binary system. **Panels (j)-(l):** csd3 passes through the circumbinary disk again and develops further by the spiral-arm accretion of the circumbinary disk. Then, csd3 becomes a highly-eccentric and wide-orbit tertiary companion of the binary system (see also Figure 4). We find that all the SPH particles of csd3 in panel (c) of Figure 1 are replenished to newly accreted SPH particles in panel (f) of Figure 1. On the other hand, the SPH particles of csd3 are scarcely replenished in the subsequent encounters with the spiral arms once the counter-rotation emerges.

Figure 2 shows the zoom-in view of the surface density around csd3 after the counter-rotation emerges. Figure 2 clearly shows that the circumstellar disk is counter-rotating. Panels (j), (k), and (l) of Figure 2 indicate that csd3 mainly accumulates the spiral-arm gas that rotates clockwise around it. The counter-rotation of csd3 is induced and enhanced by that spiral-arm gas. Therefore, we conclude that the spiral-arm accretion of the circumbinary disk is essential for the counter-rotating disk formation around the tertiary companion.

Next, let us consider the evolution of the disk rotational directions in a more quantitative fashion. For that purpose, we define the circumstellar disk as a set of SPH particles that satisfy the following three conditions: (1) gravitationally bound to the sink particle, (2) located within 100 au from the sink particle, and (3) their rotational velocity component exceeds the radial component by a factor

¹ The supplementary movie is available only in the online edition as “Supporting Information”.

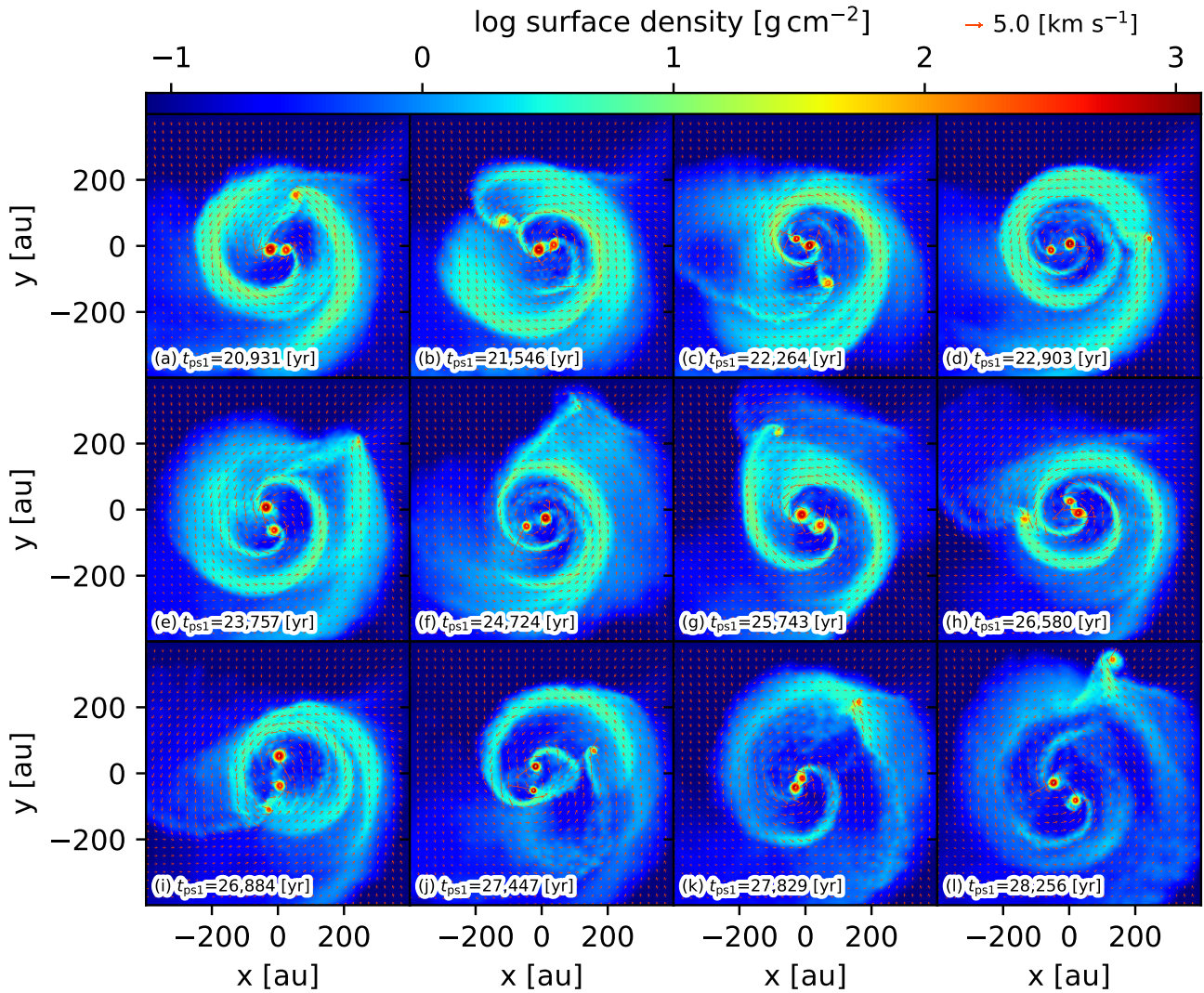


Fig. 1. Evolution of the surface density along the z -direction when the rotational direction of the tertiary circumstellar disk (csd3) is reversed. Different panels are labeled by t_{ps1} , the elapsed time after the primary protostar (ps1) formation. The origin of a coordinate system is shifted to the center of mass of the triple system. Red arrows of the panels show the density-weighted projected velocity. The length of the arrow is proportional to the velocity amplitude (the reference arrow plotted above the figure corresponds to 5 km s^{-1}).

of 2 ($|(\mathbf{v}_{\text{SPH}} - \mathbf{v}_s)_t| > 2|(\mathbf{v}_{\text{SPH}} - \mathbf{v}_s)_r|$, where \mathbf{v}_{SPH} is the velocity of the SPH particle, \mathbf{v}_s is the velocity of the sink particle, and the subscripts t and r denote the tangential and radial components of the relative velocity). We confirm that our result does not qualitatively change for other reasonable choices of the disk definition.

Using the above disk definition, we compute the angular momenta of the primary, secondary, and tertiary circumstellar disks: \mathbf{J}_{d1} , \mathbf{J}_{d2} , and \mathbf{J}_{d3} . Then, we define the disk-orbit angles relative to the inner binary orbit:

$$\psi_{\text{di-12}} = \cos^{-1} \left(\frac{\mathbf{J}_{\text{di}} \cdot \mathbf{h}_{12}}{|\mathbf{J}_{\text{di}}| |\mathbf{h}_{12}|} \right), \quad i = 1, 2, 3, \quad (1)$$

where, \mathbf{h}_{12} is the specific orbital angular momentum of the binary system of ps1 and ps2.

Figure 3 shows the time evolution of the disk-orbit angles $\psi_{\text{d1-12}}$ (blue), $\psi_{\text{d2-12}}$ (orange), and $\psi_{\text{d3-12}}$ (green) as a function of the elapsed time after the ps3 formation, $t_{\text{ps3}} (= t_{\text{ps1}} - 17,700 \text{ yr})$. First, the values of $\psi_{\text{d3-12}}$ are less than $\sim 20^\circ$ in $t_{\text{ps3}} \lesssim 4 \times 10^3 \text{ yr}$. Then, $\psi_{\text{d3-12}}$ begins to oscillate in $4 \times 10^3 \text{ yr} \leq t_{\text{ps3}} \leq 10^4 \text{ yr}$. Finally, $\psi_{\text{d3-12}}$ has values of $\gtrsim 160^\circ$ in $t_{\text{ps3}} \gtrsim 10^4 \text{ yr}$, meaning that the rotational direction of csd3 is almost antiparallel with that of the orbital motion of the binary system. All the values of $\psi_{\text{d1-12}}$ and $\psi_{\text{d2-12}}$ are less than 13° in $t_{\text{ps3}} \lesssim 6.4 \times 10^4 \text{ yr}$, meaning that the rotational direction of csd1 and csd2 are both well aligned with that of the orbital motion of the binary system. The results clearly show that csd3 is counter-rotating with respect to csd1, csd2, and their orbital motion. The counter rotation of csd3 continues from $t_{\text{ps3}} = 10^4 \text{ yr}$

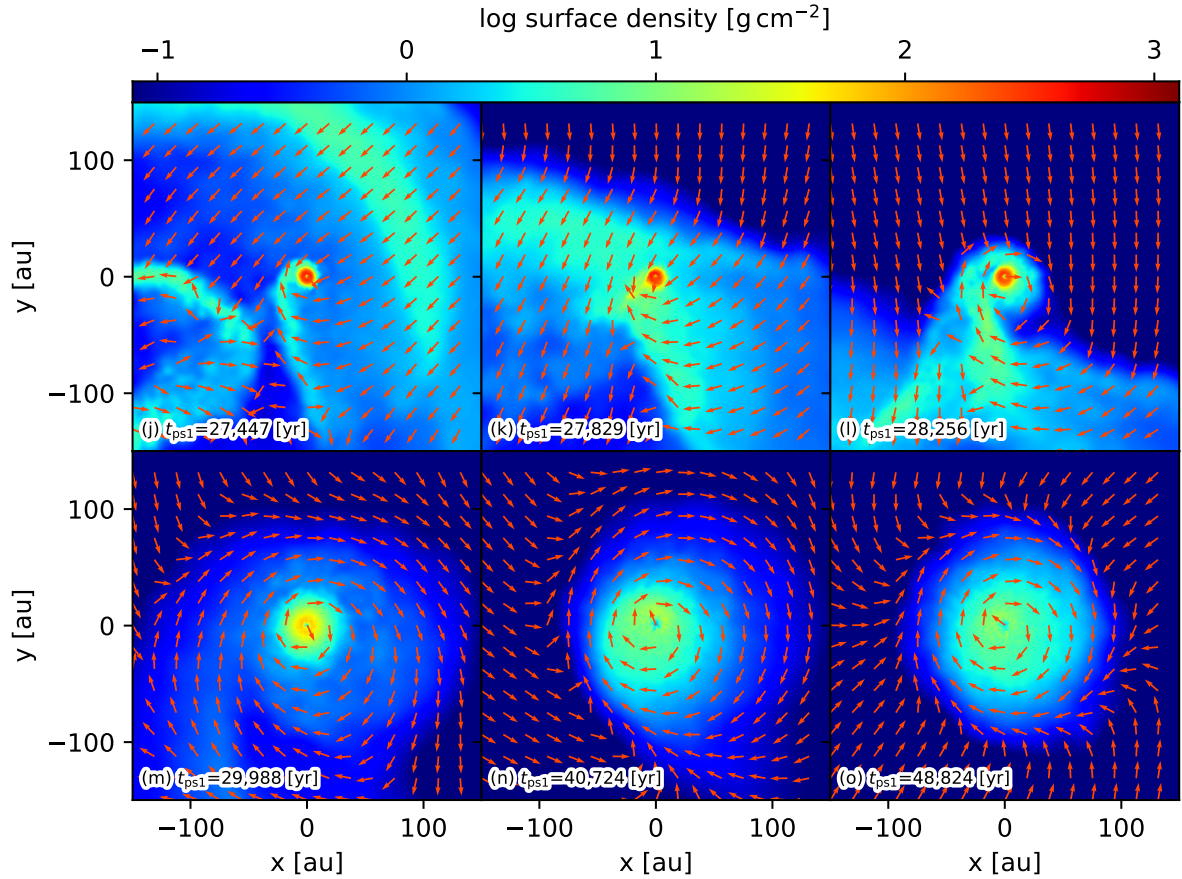


Fig. 2. Zoom-in view of the evolution of the surface density along the z -direction. The origin of a coordinate system is shifted to the position of ps3. Red arrows show the directions of the density-weighted projected velocity in the rest frame of ps3. The lengths of the arrows are the same and independent of its velocity amplitude. Panels (j), (k), and (l) correspond to panels (j), (k), and (l) in Figure 1.

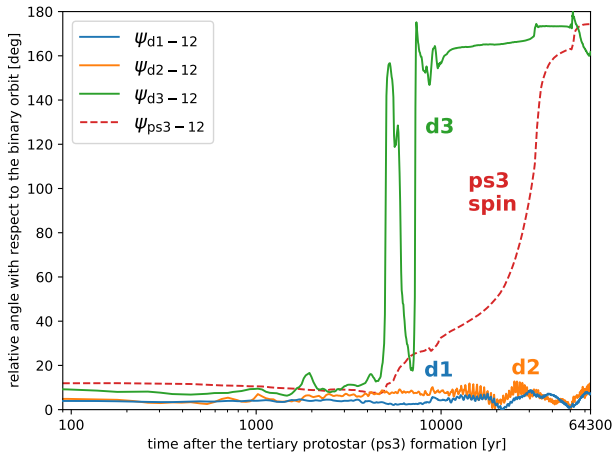


Fig. 3. Evolution of the disk-orbit angles ψ_{d1-12} (blue), ψ_{d2-12} (orange), and ψ_{d3-12} (green) as a function of t_{ps3} that is the elapsed time after ps3 formation. Red dashed line shows the evolution of the star-orbit angle ψ_{ps3-12} .

to $t_{ps3} = 6.4 \times 10^4$ yr. Therefore, we are left with a counter-rotating disk that is stable at least more than $\sim 5 \times 10^4$ yr.

Figure 3 also shows the time evolution of the star-orbit angle ψ_{ps3-12} that is the relative angle between the stellar spin axis of ps3 and the orbital axis of the inner binary system represented by \mathbf{h}_{12} . The stellar spin axis of ps3 is initially well aligned with the binary orbital axis, and therefore with the rotation axis of csd3 as well. Even when csd3 reverses its rotation axis, the stellar spin axis of ps3 remains the same for a while. However, the stellar spin axis of ps3 gradually becomes aligned with the disk rotation axis through the circumstellar disk accretion to ps3. Finally, the star-disk angle of the tertiary system becomes less than $\sim 20^\circ$, i.e., $\psi_{ps3-12} \approx \psi_{d3-12}$. We confirm that the stellar spin axes of ps1 and ps2 are always well aligned with their orbital axis within $\sim 15^\circ$.

Therefore, the present formation scenario of the counter-rotating disk does not lead to the star-disk misalignment, which can cause the spin-orbit misalignment often observed for transiting exoplanetary systems (e.g., Ohta et al. 2005; Xue et al. 2014; Winn & Fabrycky 2015;

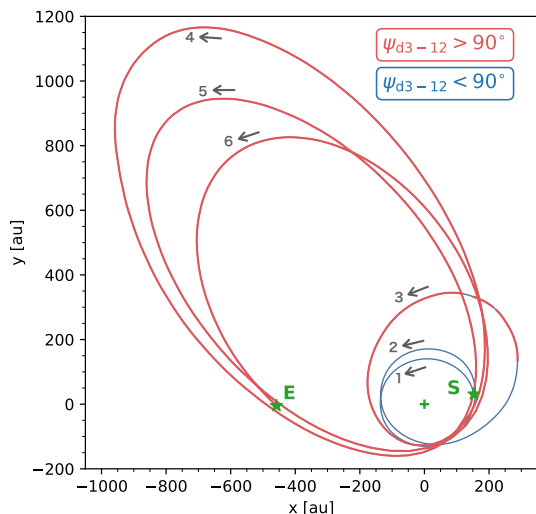


Fig. 4. Trajectory of the tertiary with respect to the center of mass of the inner binary system ($x = y = 0$). The symbols S and E mark the positions of csd3 at its formation epoch and at the end of the simulation. Blue and red lines represent the trajectories where $\psi_{d3-12} < 90^\circ$ and $\psi_{d3-12} > 90^\circ$, respectively.

Kamiaka et al. 2019).

Figure 4 plots the trajectory of the tertiary with respect to the center of mass of the inner binary on the x - y plane. The initially circular orbit becomes eccentric after a few orbital periods, and its semi-major axis remarkably increases. The eccentric orbit of the tertiary plays an essential role in our spiral-arm accretion scenario for the counter-rotating disk formation. We find that the triple system satisfies the dynamical instability condition (Mardling & Aarseth 2001) just before the onset of the eccentric orbit. Furthermore, the triple system remains unstable and is still evolving by the hydrodynamical disk interaction and envelope accretion after the counter-rotation emerges. Thus, the orbit instability of the tertiary may be mainly triggered by the gravitational three-body effect, while the hydrodynamical disk interaction and envelope accretion are also influential in its subsequent evolution.

Figure 5 schematically summarizes our formation scenario of the counter-rotating disk. The presence of the circumbinary disk and the eccentric orbital evolution of the tertiary are the two essential ingredients for the efficient spiral-arm accretion.

Kurtovic et al. (2018) discovered a hierarchical triple system HT Lup: a close (25 au) binary system HT Lup A-B with counter-rotating twin disks has a wide-separation companion HT Lup C located at 434 au away. Interestingly, the architecture of HT Lup seems to be similar to the architecture illustrated in Figure 5.

Finally, Figure 6 shows the density-weighted line-of-sight velocity viewed from the y -axis of Figure 1(i).

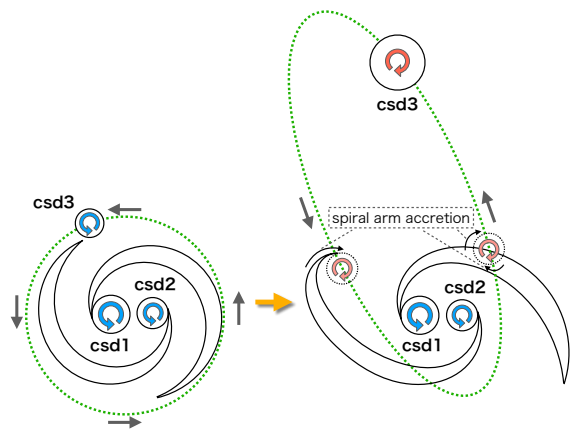


Fig. 5. Schematic illustration of the spiral-arm accretion scenario for the counter-rotating disk formation.

The blueshifted and redshifted velocity structures of the three circumstellar disks appear to be consistent with the Keplerian rotating disk with the infalling envelope (Momose et al. 1998). The velocity pattern of the blueshifted to redshifted components of csd3 (left) is almost opposite to that of csd1 (lower right) and csd2 (upper right), indicating that the projected rotational direction of csd3 is close to antiparallel with that of csd1 and csd2. Indeed, this velocity pattern is similar to observed counter-rotating disks (Kurtovic et al. 2018; Tanaka et al. 2020; Ichikawa et al. 2021).

4 Conclusion and discussion

The new formation pathway of the counter-rotating disk (see Figure 5) is summarized as follows; (i) a tertiary protostar forms via the fragmentation of the circumbinary disk, (ii) the tertiary orbit becomes unstable due to the three-body effect and acquires a large eccentricity, (iii) the circumstellar disk of the tertiary orbit receives the counter-rotating gas accretion when crossing the spiral-arm of the circumbinary disk, and its rotational direction is reversed. This scenario works on the basis of gravito-hydrodynamical processes alone and does not require more complicated physical processes such as the magnetic field. The material of the counter-rotating disk is entirely newly accreted, and it is scarcely replenished in the subsequent encounters with the spiral arms once the counter-rotating disk forms.

The occurrence rate of the found formation pathway is still unclear so far. The counter-rotating disk is formed when the angular momentum of the accreting fluid elements from the spiral arm to the tertiary is reversed in the rest frame of the tertiary protostar. This process occurs when the tertiary passes through the backside of the spiral arm. Thus, it is crucial that whether the passing-through-

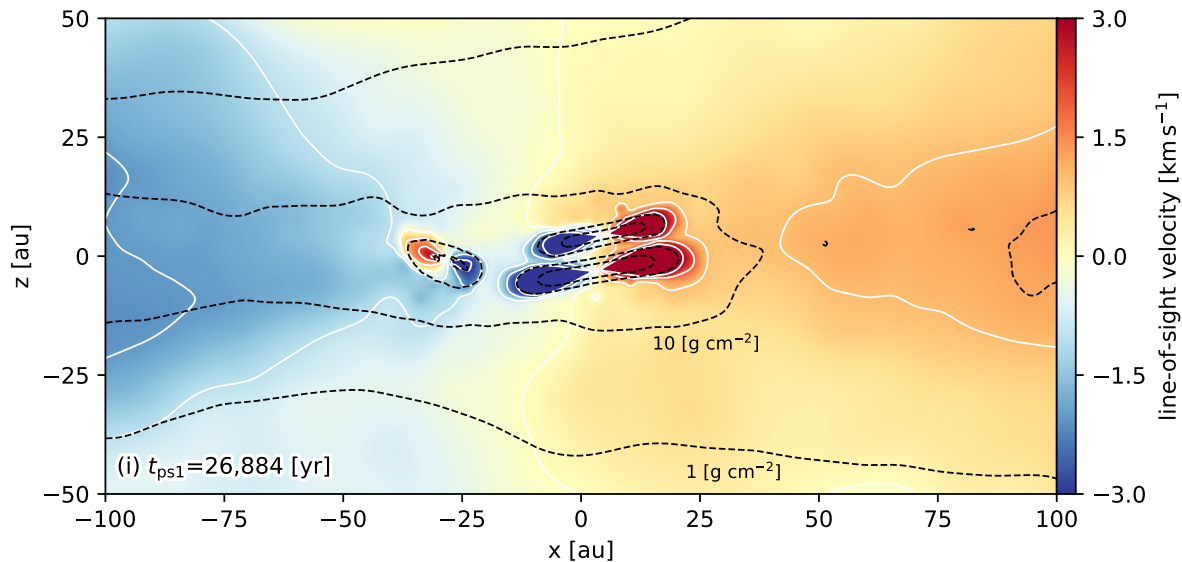


Fig. 6. Density-weighted line-of-sight velocity viewed from the y -direction at $t_{ps1} = 26,884$ yr corresponding to panel (i) of Figure 1. The origin of a coordinate system is shifted to the center of mass of the triple protostar system. White solid lines represent the contours of the density-weighted line-of-sight velocity from -3 km s^{-1} to $+3 \text{ km s}^{-1}$ in steps of 1 km s^{-1} . Black dashed lines are the contours of the surface density at 1 g cm^{-2} , 10 g cm^{-2} , 10^2 g cm^{-2} , and 10^3 g cm^{-2} from outer to inner regions. The integrations of y -direction are taken from -400 au to $+400 \text{ au}$ (i.e., the size of the panel (i) of Figure 1).

the-back-side-of-spiral-arm occurs by chance or with a relatively high probability to clarify whether the formation of the counter-rotating disk is rare or not.

The qualitative idea for the counter-rotating disk formation is speculated as follows. The tertiary system is formed in the circumbinary disk, and its orbital period is roughly the same as that of its natal circumbinary disk even after the tertiary orbit becomes eccentric. Thus, the tertiary is expected to be in a 1:1 resonance with the spiral arms of the circumbinary disk. Therefore, it is speculated that the passing-through-the-back-side-of-spiral-arm occurs in the course of the multiple encounters. This qualitative idea for the counter-rotating disk formation will be examined in the follow-up studies.

Another question is how long the counter-rotating disk survives the subsequent evolution. The triple system is still unstable due to the three-body effect and evolving by the hydrodynamical disk interaction and envelope accretion after the counter-rotating disk formation. For instance, recent theoretical studies suggest that the disk rotational direction can dynamically change by the envelope accretion that has the random gas motion by the turbulence (Tsukamoto & Machida 2013) and by the tidal interaction between the binary pair (Matsumoto et al. 2015). However, we can not currently address the long-term prospects for the stability and survivability of this system from the data we have. The long-term prospects for stability and survivability will be also given in the follow-up studies.

The remaining questions are crucial to understand if our proposed scenario can be a major formation channel for a variety of counter-rotating and misaligned disk systems recently discovered by ALMA.

Supporting Information

Additional Supporting Information is available in the online version of this article: The supplementary movie 1.

Acknowledgments

We are grateful to the anonymous referee for the fruitful suggestions and insightful comments that helped to improve the manuscript. Numerical computations were carried out on Cray XC50 at Center for Computational Astrophysics, National Astronomical Observatory of Japan. This research is supported by the Japan Society for the Promotion of Science (JSPS) Core-to-Core Program “International Network of Planetary Sciences”, and by JSPS KAKENHI Grant Numbers JP18H01247 (Y.S.), JP18H05437 (Y.T.), JP18K13581 (Y.T.), JP19H01947 (Y.S.), and JP21J23102 (D.T.). The supplementary movie was produced using SPLASH (Price 2007).

References

- Adams, F. C., Ruden, S. P., & Shu, F. H. 1989, *ApJ*, 347, 959
- Alves, F. O., Caselli, P., Girart, J. M., Segura-Cox, D., Franco, G. A. P., Schmiedeke, A., & Zhao, B. 2019, *Science*, 366, 90
- Bate, M. R., Bonnell, I. A., & Price, N. M. 1995, *MNRAS*, 277, 362
- Bonnell, I. A. & Bate, M. R. 1994, *MNRAS*, 271, 999
- Brinch, C., Jørgensen, J. K., Hogerheijde, M. R., Nelson, R. P., & Gressel, O. 2016, *ApJ*, 830, L16

- Burkert, A. & Bodenheimer, P. 2000, *ApJ*, 543, 822
- Fisher, R. T. 2004, *ApJ*, 600, 769
- Ichikawa, T., Kido, M., Takaishi, D., Shimajiri, Y., Tsukamoto, Y., & Takakuwa, S. 2021, arXiv e-prints, arXiv:2106.11924
- Jensen, E. L. N. & Akeson, R. 2014, *Nature*, 511, 567
- Kamiaka, S., Benomar, O., Suto, Y., Dai, F., Masuda, K., & Winn, J. N. 2019, *AJ*, 157, 137
- Kraus, S., Kreplin, A., Young, A. K., Bate, M. R., Monnier, J. D., Harries, T. J., Avenhaus, H., Kluska, J., Laws, A. S. E., Rich, E. A., Willson, M., Aarnio, A. N., Adams, F. C., Andrews, S. M., Anugu, N., Bae, J., ten Brummelaar, T., Calvet, N., Curé, M., Davies, C. L., Ennis, J., Espillat, C., Gardner, T., Hartmann, L., Hinkley, S., Labdon, A., Lanthermann, C., LeBouquin, J.-B., Schaefer, G. H., Setterholm, B. R., Wilner, D., & Zhu, Z. 2020, *Science*, 369, 1233
- Kurtovic, N. T., Pérez, L. M., Benisty, M., Zhu, Z., Zhang, S., Huang, J., Andrews, S. M., Dullemond, C. P., Isella, A., Bai, X.-N., Carpenter, J. M., Guzmán, V. V., Ricci, L., & Wilner, D. J. 2018, *ApJ*, 869, L44
- Mardling, R. A. & Aarseth, S. J. 2001, *MNRAS*, 321, 398
- Matsumoto, T., Onishi, T., Tokuda, K., & Inutsuka, S. I. 2015, *MNRAS*, 449, L123
- Momose, M., Ohashi, N., Kawabe, R., Nakano, T., & Hayashi, M. 1998, *ApJ*, 504, 314
- Offner, S. S. R., Kratter, K. M., Matzner, C. D., Krumholz, M. R., & Klein, R. I. 2010, *ApJ*, 725, 1485
- Ohta, Y., Taruya, A., & Suto, Y. 2005, *ApJ*, 622, 1118
- Price, D. J. 2007, *PASA*, 24, 159
- Takaishi, D., Tsukamoto, Y., & Suto, Y. 2020, *MNRAS*, 492, 5641
- Takakuwa, S., Saigo, K., Matsumoto, T., Saito, M., Lim, J., Hanawa, T., Yen, H.-W., & Ho, P. T. P. 2017, *ApJ*, 837, 86
- Tanaka, K. E. I., Zhang, Y., Hirota, T., Sakai, N., Motogi, K., Tomida, K., Tan, J. C., Rosero, V., Higuchi, A. E., Ohashi, S., Liu, M., & Sugiyama, K. 2020, *ApJ*, 900, L2
- Tsukamoto, Y. & Machida, M. N. 2013, *MNRAS*, 428, 1321
- Winn, J. N. & Fabrycky, D. C. 2015, *ARA&A*, 53, 409
- Xue, Y., Suto, Y., Taruya, A., Hirano, T., Fujii, Y., & Masuda, K. 2014, *ApJ*, 784, 66